JOURNAL OF MATERIALS SCIENCE 23 (1988) 1379–1384

Control of the continuous rheocasting process

Part 1 *Heat flow model*

M. A. TAHA, N. A. EL-MAHALLAWY, A. M. ASSAR
Department of Mechanical Design and Production Engineering, Faculty of Engineering, Ain-Shams University, Abasia, Cairo, Egypt

In the continuous rheocasting process, a semi-solid alloy is obtained from the exit port of the apparatus at a given rate and with a given fraction of solid. This solid fraction is dependent on the corresponding temperature within the solid–liquid range which should be controlled accurately by the process parameters for a given rheocaster stirring chamber. For this purpose a heat flow model has been established for the continuous rheocasting of Bi–17 wt% Sn alloy. The heat transfer calculations are based on the solution of the two-dimensional partial differential equations using a finite difference method. An excellent agreement between calculations and experimental results is found. Computations are carried out in order to find the influence of stirring chamber dimensions on the alloy exit temperature and therefore, the volume fraction of solid. The influence of input metal temperature and metal flow rate on the exit temperature and volume fraction of solid are also found.

1. Introduction

During the last decade, considerable research work has been directed towards the improvement of alloy properties in the as-cast condition by applying some innovative casting processes [1, 2].

One of the processes which shows remarkable improvement in soundness, homogeneity and structure is the rheocasting (or stir-casting) process. Research on this process was started by Spencer *et al.* [3] in 1972. The process consists of vigorously agitating the alloy in the solid–liquid temperature range, to produce a highly fluid semi-solid slurry, which is then cast at a temperature between the liquidus and solidus. There are two techniques, either batch-type or continuous-type rheocasting. The continuous type is the more promising in practice [4].

Many publications have appeared on the process, studying slurry rheological behaviour and as-cast properties such as soundness, structure, homogeneity, mechanical properties and deformability [4–12]. These publications indicate many promising aspects of the process and the as-cast properties. However, the application of the process on an industrial scale is still very limited due to the difficulty in controlling the process parameters.

The present work is a contribution to solving this problem and is divided in two parts: the present paper and a second one on the rheological behaviour analysis. The research plan includes all the steps needed for producing a continuous flow of alloy slurry with a given volume fraction of solid, G_s. These steps are illustrated by the flow diagram shown in Fig. 1. In this paper a heat transfer model, which gives the temperature gradient produced in Bi–17 wt % Sn alloy contained inside a continuous rheocaster, is presented. The influence of rheocaster dimensions and other process variables on the temperature of the slurry thus produced is obtained.

2. Experimental set-up

The continuous rheocaster (Fig. 2) consists mainly of an upper cylindrical crucible made of austenitic cast iron and a lower smaller cylindrical stirring chamber located on the same axis. The upper chamber (crucible) has 175 mm internal diameter and 240 mm height while the lower chamber (stirring chamber) has 39.6 mm internal diameter and 200 mm height. Four electrical resistance coils of 4 kW are used to heat the upper chamber. These coils are connected to a transformer with a built-in temperature controller to regulate the temperature inside the chamber within ± 2 K. Additional resistance coils, used to heat the stirring chamber, are also connected to another transformer with a temperature controller. The temperature of the air-gap existing between the coils and the stirring chamber was also controlled within ± 2 K. At the same time a cooling coil (copper tube) is installed around the stirring chamber and connected to a water bath with a digital temperature controller, where the temperature was controlled within ± 0.1 K. The heating and cooling coils were used to produce an appropriate temperature gradient in the alloy along the axis of the stirring chamber. The value of the temperature gradient will determine the temperature and consequently the volume fraction of solid at the exit port. Metal flow through this port was controlled by the vertical position of the stirrer, which is a stainless steel bar (35.6 mm in diameter and 510 mm long) with a hemispherical lower end. The lower part of the stirrer which is inserted in the stirring chamber has a special shape in order to get an efficient agitation. The stirrer was powered by a 1.8 kW, 3000 r.p.m. d.c. motor

0022–2461/88 $03.00 + .12

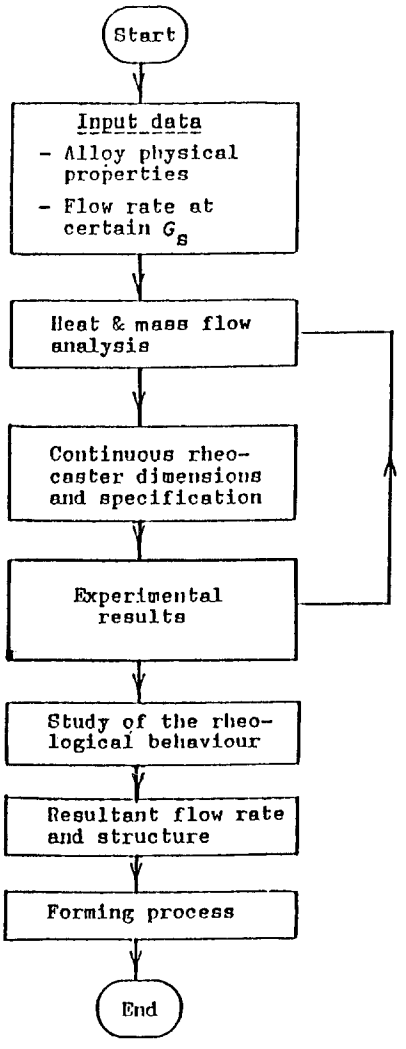

Figure 1 Flow diagram for producing required slurry continuously.

connected to a speed control unit to achieve a constant speed during the variation of the torque. The alloy was solidified gradually during its downward flow in the stirring chamber, while it is subjected to vigorous agitation provided by the stirrer. To prevent the freezing of the alloy below the exit port in the case of non-continuous flow, an additional resistance heater was placed at the exit port of the rheocaster to heat its vicinity to a temperature equal to the exit temperature of the slurry to within 5 K. Five chromel–alumel thermocouples were set in the wall of the stirring chamber along its height and were connected to a five-channel chart recorder.

3. Rheocasting experiments

Before starting the process, the charge in the upper and middle chamber was heated to a temperature above the liquidus by various superheats ranging between 15 to 45 K. After complete melting, the stirrer was set in motion at the desired speed. The power in the bottom coil was set so as to keep the exit nozzle temperature at the appropriate level. Once the slurry temperature had reached the required level and consequently the desired volume of solid fraction, the stainless steel stirrer was raised from the exit port and the slurry started flowing out. The flow rate was controlled by adjusting the position of the stirrer inside the stirring chamber. The amount of heat extracted from the

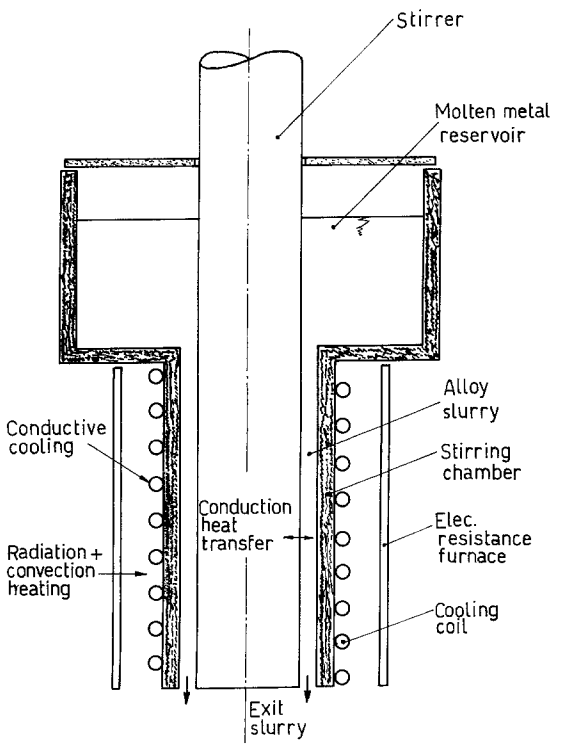

Figure 2 Schematic representation of continuous rheocaster.

stirring chamber was controlled by the input temperature of the cooling water and the temperature of the controlled furnace (consequently the atmospheric temperature around the cooling coil). Since the amount of heat was kept constant, therefore the volume fraction of solid at the exit port of the stirring chamber was inversely proportional to the flow rate and input temperature. During the flow of metal slurry in the stirring chamber, the input temperature was kept above the liquidus. Once the thermocouple readings indicated that a steady state had been reached, the metal slurry was quenched in a cooled copper mould (4 g) with a cylindrical cavity (8 mm diameter, 8 mm height).

4. Heat flow model

In the continuous rheocasting, the molten metal flows from the reservoir and enters the stirring chamber (Fig. 2). The stirring chamber is subjected to radiative heat from the furnace, natural convection from the air present in the furnace–chamber gap, and to conductive cooling by the cooling coils. At the bottom of the stirring chamber, a resistance furnace is present to keep the temperature of the atmosphere equal to the exit temperature of the slurry. As the stirring action is mainly circumferential, therefore axial convection is assumed to be negligible and heat flow is considered to be by conduction only in both liquid and semi-solid states. The melt flows downwards in the stirring chamber with a constant speed, so that a steady-state condition is reached and the process can be considered similar to steady-state continuous casting, described by the following partial differential equation:

$$K\left[\frac{d^2T}{dz^2}+\frac{d^2T}{dr^2}+\left(\frac{1}{r}\right)\frac{dT}{dr}\right]+q-c_pV\left(\frac{dT}{dz}\right)=0 \quad (1)$$

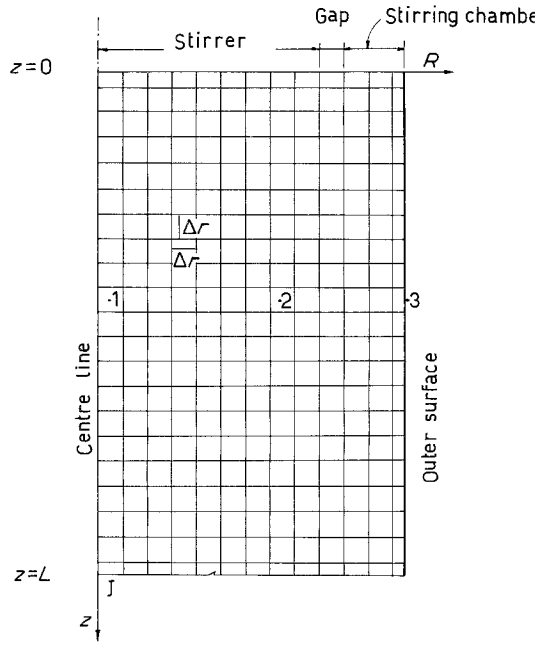

Figure 3 The mesh points and their positions used in the computations.

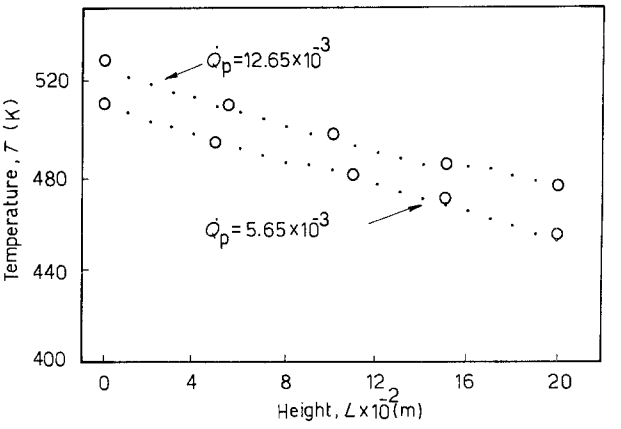

Figure 4 (○) Experimental and (·) calculated temperature distribution of Bi–17 wt % Sn slurry along the height of stirring chamber at flow rates 5.65 × 10^{-3} and 12.65 × 10^{-3} kg sec^{-1}, the shear rate being 270 sec^{-1}.

where K is the thermal conductivity, T is the temperature, z and r the axial and radial coordinates respectively, c_p the specific heat and V the axial displacement velocity of the slurry. q corresponds to the evolution of latent heat due to the change of phase and is given by the equation

$$q = \text{latent heat} \times V(dG_s/dz) \quad (2)$$

The boundary conditions are:

$$\text{at } z = 0 \qquad T = T_i,\ dT/dz = 0$$

$$\text{at } z = L \qquad dT/dz = 0$$

$$\text{at } R = 0 \qquad dT/dr = 0$$

$$\text{at } R = R_2 \qquad dT/dr = Q,\ d^2T/dr^2 = 0$$

where Q is the net conductive, convective and radiative heat flux.

4.1. Method of solution

Equation 1 is solved using the finite difference method. A network is placed on the longitudinal section as shown in Fig. 3. The set of linear equations is solved using the Gauss–Seidel iterative method [13]. The iterations are stopped when the error is less than 0.1 K. In order to speed up the iteration, an over-relaxation factor OMEGA = 1.1 was used.

4.2. Determination of thermal parameters

The thermal conductivity of the liquid metal K_L and of the mixture of liquid plus solid K_S are calculated using the linear Rule of Mixtures, and the conductivities of the liquid pure metal and that of the solid phases whenever present. It is to be noted that the conductivities of the two phases are very close to each other (K_L = 10.1 W m^{-1}K^{-1}, K_S = 10.2 W m^{-1}K^{-1}). The thermal and physical properties of the alloy used in the computations are given in Table I. Some thermal resistances are needed for the computations, namely the resistance between the copper and the outer surface of the stirring chamber, ETA, the resistance between the alloy slurry and the inner surface of the stirring chamber, GAMMA, and the resistance between the alloy slurry and the stirrer, PHI. A comparison between the experimental and computed results is made in terms of the temperature distribution along the axis of the stirring chamber for different flow rates, ranging between 4.85 × 10^{-3} and 14.6 × 10^{-3} kg sec^{-1} and for four different shear rates of 270, 450, 675 and 900 sec^{-1}. A sample of these results is shown in Fig. 4, where an excellent agreement between computation and experiments are found for the heat resistances ETA = 0.001 m^{2}K W^{-1}, GAMMA = PHI = 0 m^{2}K W^{-1}. These values are reasonable since a thermal resistance exists between the outer surface of the stirring chamber and the copper cooling tube while no resistance exists between the slurry and both the stirrer and stirring chamber.

5. Effect of stirring chamber dimensions on exit temperature

The dimensions of the stirring chamber which have the main effect on the exit temperature and the corresponding volume of solid fraction are the height of the stirring chamber and the number of cooling coils per unit height of the stirring chamber, i.e. the rate of heat

TABLE I Physical properties of Bi–17 wt % Sn alloy [14, 15]

Thermal conductivity of the liquid alloy (T = 486 to 573 K)	10.1 W m^{-1}K^{-1}
Thermal conductivity of the solid alloy (T = 486 to 433 K)	10.2 W m^{-1}K^{-1}
Density of the alloy	0.0093 kg m^{-3}
Latent heat of fusion	39 501 JK^{-1}g^{-1}
Liquidus temperature	486 K
Solidus temperature	412 K
Specific heat	180.4 J kg^{-1}K^{-1}

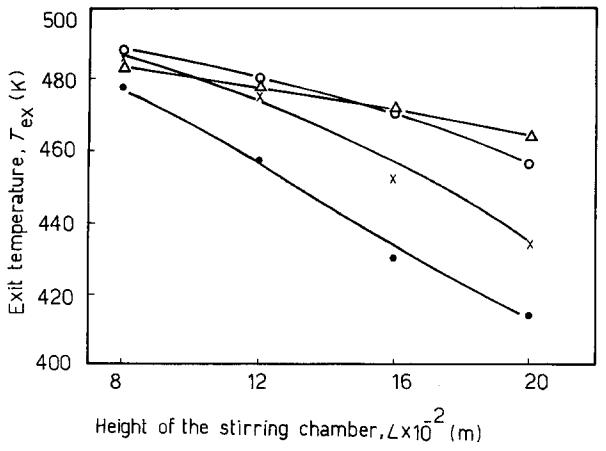

Figure 5 Effect of stirring chamber height on the exit temperature and the corresponding volume fraction of solid. (●) 500 K, (x) 510 K, (○) 520 K, (△) 530 K.

extraction. As the cooling rate is slow in the stirring chamber the solidification of the alloy is considered to be under equilibrium conditions, and the phase distribution in the mushy zone can be calculated using the lever rule. The relation between the temperature T and fraction of solid G_s is given by

$$G_s = 1 - \frac{48.5}{261.5 - T} \quad (3)$$

The effect of the height of the stirring chamber, L, on the exit temperature T_{ex} is shown in Fig. 5. At the same number of cooling coils per unit height, and flow rate, and at different values of input temperatures T_i, the exit temperature decreases with increasing height L. This result is reasonable since the amount of heat extracted from the outer surface of the stirring chamber, Q_n, increases with the height L. The effect of the number of cooling coils per unit height, N_g, on T_{ex} and the corresponding G_s and the cooling rate $\dot{\varepsilon}$ is shown in Fig. 6. The exit temperature decreases gradually with increasing N_g from 50 to 60, above which it decreases rapidly. The corresponding solid fraction G_s at the exit port increased from 0.39 to 0.58 by increasing N_g from 50 to 80. As the primary cooling rate has the major effect on the structure of the rheocast material it is found that $\dot{\varepsilon}$ increases from 8 to

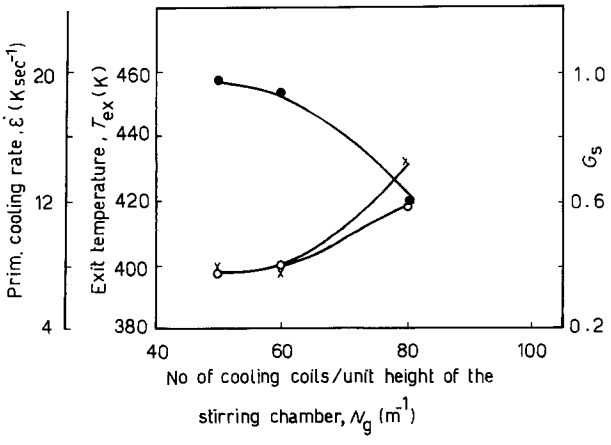

Figure 6 Effect of number of cooling coils per unit height around stirring chamber on (●) exit temperature, (○) corresponding volume fraction of solid and (x) cooling rate.

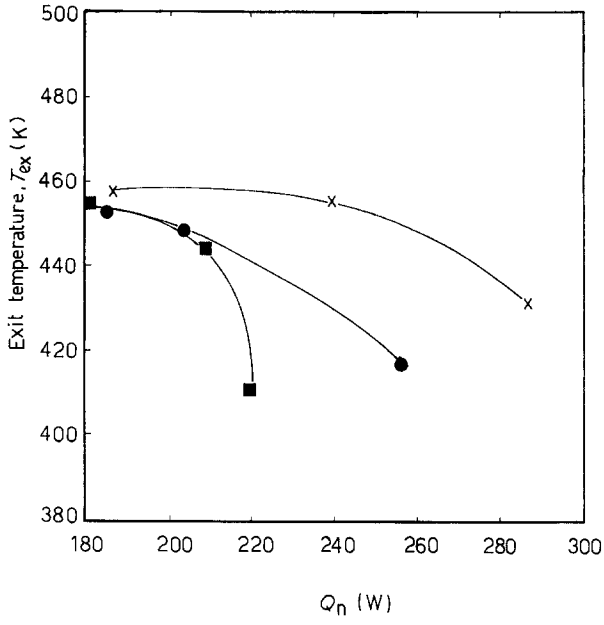

Figure 7 Effect of heat extracted from outer surface of stirring chamber on T_{ex}. Q_p = (■) 4 × 10^{-3}, (●) 9 × 10^{-3}, (x) 13 × 10^{-3} kg sec^{-1}.

14.5 K sec^{-1} as N_g increases from 50 to 80. This behaviour is reasonable as the rate of heat extraction increases with N_g at a given flow rate.

Fig. 7 shows the effect of rate of heat extraction Q_n on the exit temperature at different flow rates. The curves in Fig. 7 show a relatively slower rate of temperature drop at higher exit temperatures followed by a higher rate. This is due to the different rates of latent heat evolved which are higher at temperatures closer to the liquidus than to the solidus (see Equation 3). Fig. 7 also indicates that as the flow rate increases, higher rates of heat extraction should be achieved to reach a given exit temperature, which is a reasonable result.

6. Effect of input temperature and metal flow rate on the exit temperature and the corresponding solid fraction

Fig. 8 shows the effect of input temperature T_i on the exit temperature, volume fraction of solid and the primary cooling rate. Increasing T_i from 500 to 530 K leads to an almost similar increase of T_{ex} from 447 to 472 K, and therefore a corresponding decrease in G_s from 0.44 to 0.22 as well as a decrease in the cooling rate from 9.1 to 3.55 K sec^{-1}.

Fig. 9 shows the effect of metal flow rate Q_p on T_{ex}, G_s and $\dot{\varepsilon}$. Increasing the flow rate leads to increasing both T_{ex} and $\dot{\varepsilon}$ and to decreasing G_s. From the figure it is observed that increasing Q_p from 1 × 10^{-3} to 13 × 10^{-3} kg sec^{-1} results in the increasing of T_{ex}.

7. Practical significance

The assessment of a heat flow model based on the solution of the steady-state conduction equation is found successfully applicable to the continuous rheocaster. The results of the model are important in the design of the rheocaster, thus reducing time and material losses during operation.

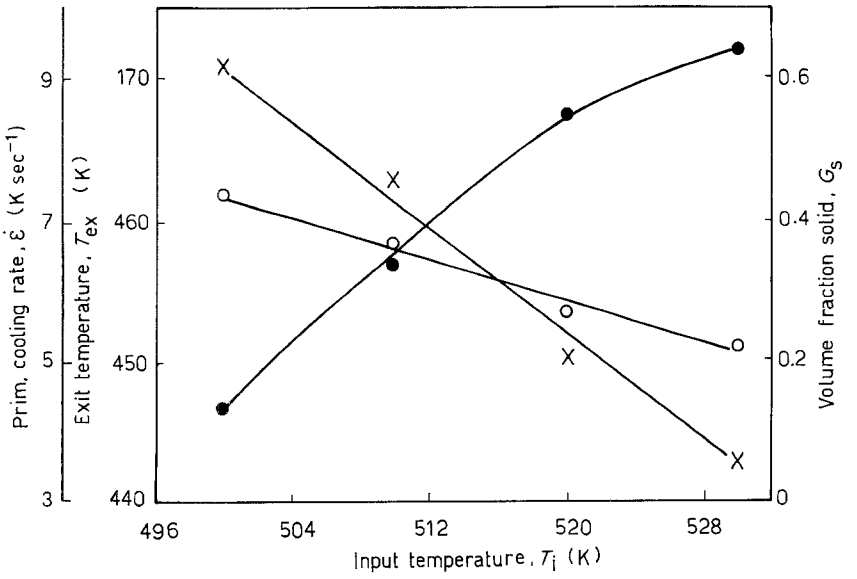

Figure 8 Effect of input temperature on (●) exit temperature, (○) corresponding volume fraction of solid and (x) cooling rate at $L = 0.2\,\text{m}$, $Q_p = 9 \times 10^{-3}\,\text{kg sec}^{-1}$ and $N_g = 50\,\text{m}^{-1}$.

The dimensions of the stirring chamber, the number of cooling coils and the specifications of heaters are first determined for a required range of exit temperature and maximum flow rates for a given alloy or alloys. During operating the rheocaster, the process variables can be readjusted based on the results of the model. Moreover, a cooling rate can be calculated from the model which can be used to predict the size of the microstructural parameters [16].

8. Conclusions

From the above results and discussions the following conclusions can be drawn: The slurry exit temperature and corresponding G_s, are mainly affected by the melt input temperature, T_i, and the number of cooling coils per unit height of the stirring chamber, N_g. It is also affected by the slurry flow rate, Q_p, and the height of the stirring chamber, L. The exit temperature increases with increasing T_i and Q_p, and decreasing N_g and L.

Acknowledgements

The authors acknowledge financial support by the Egyptian Student Mission and Giesserei-Institut der RWTH, Aachen, at which the experimental part of this work was done. They wish to thank Professor A. S. El-Sabagh of Ain-Shams University and Professor Peter R. Sahm for their contributions.

References

1. N. A. EL-MAHALLAWAY and M. A. TAHA, *J. Metals* **37** (9) (1985) 42.
2. M. A. TAHA and N. A. EL-MAHALLAWY, in "Mechanical Behavior of Materials III", Proceedings of 3rd International Conference (ICM3), Cambridge, UK, 1979, Vol. 2, edited by K. J. Muller and R. F. S. Smith (Pergamon, 1980) p. 537.
3. D. B. SPENCER, R. MEHRABIAN and M. C. FLEMINGS, *Met. Trans.* **3** (1972) 1925.
4. M. C. FLEMINGS, R. G. RIEK and K. P. YOUNG, *Mater. Sci. Eng.* **25** (1976) 103.
5. P. A. JOLY and R. MEHRABIAN, *J. Mater. Sci.* **11** (1976) 1393.
6. A. M. ASSAR, N. A. EL-MAHALLAWY and M. A. TAHA, *Aluminium* **57** (1981) 807.
7. *Idem, Met. Technol.* **9** (1982) 165.
8. A. EL-SAWY, N. A. EL-MAHALLAWY and M. A. TAHA, in Proceedings of 7th International Light Metal Congress, Leoben-Wien, 1981 (7th ILMT Congress Bureau, Montan University, Austria, 1981) pp. 114.
9. A. EL-MAHALLAWY, N. FAT-HALLA and M. A. TAHA, in "Mechanical Behavior in Material IV", Proceedings of the 4th International Conference, Stockholm, August 1983, Vol. 2, edited by J. Carlson and N. G. Ohlson (Pergamon, 1984) p. 695.
10. M. C. FLEMINGS and R. MEHRABIAN, "New Trends in Materials Processing" (ASM, Metal Park, Ohio, 1976) p. 98.
11. M. A. TAHA and N. A. EL-MAHALLAWY, in "Advanced Technology of Plasticity", Proceedings of 1st International Conference on Technology of Plasticity, Tokyo, 1984, Vol. 1 (Japan Society for Technology of Plasticity and

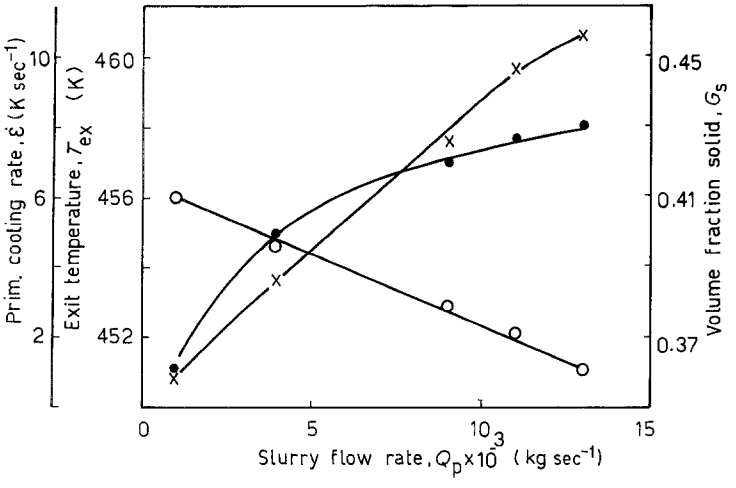

Figure 9 Effect of metal flow rate on (●) exit temperature, (○) corresponding volume fraction of solid and (x) cooling rate at $L = 0.2\,\text{m}$, $T_i = 510\,\text{K}$ and $N_g = 50\,\text{m}^{-1}$.

Japan Society of Precision Engineering, Tokyo, 1984) p. 50.
12. M. A. TAHA and M. SUERY, *Met. Technol.* **11** (1984) 226.
13. G. E. FORSYTHE and W. R. WARSOW, "Finite Difference Methods for Partial Differential Equations" (Wiley, New York, 1959).
14. C. Y. HO and R. E. TAYLOR (eds), "Thermophysical Properties of Matter", Vol. 1 (Plenum, New York, 1969) p. 511.
15. *Idem, ibid.*, Vol. 4 (1972) p. 22.
16. M. A. TAHA, N. A. EL-MAHALLAWY and A. M. ASSAR, Paper no. 136-a, in Proceedings of Conference on Solidification Processing, September 1987, Sheffield, UK, pp. 431–4.

Received 28 May
and accepted 17 August 1987